

# A wave equation migration method for receiver function imaging:

## 1. Theory

Ling Chen

Seismological Laboratory, Institute of Geology and Geophysics, Chinese Academy of Sciences, Beijing, China

Lianxing Wen

Department of Geosciences, State University of New York at Stony Brook, Stony Brook, New York, USA

Tianyu Zheng

Seismological Laboratory, Institute of Geology and Geophysics, Chinese Academy of Sciences, Beijing, China

Received 1 February 2005; revised 14 July 2005; accepted 19 August 2005; published 23 November 2005.

[1] A wave equation-based poststack depth migration method is proposed to image the Earth's internal structure using teleseismic receiver functions. By utilizing a frequency wave number domain one-way phase screen propagator for wave field extrapolation in the migration scheme, common conversion point (CCP) stacked receiver functions are backward propagated to construct a subsurface structural image. The phase screen propagator migration method takes into account the effects of diffraction, scattering, and travel time alternation caused by lateral heterogeneities, and therefore it is particularly useful for imaging complex structures and deep discontinuities overlain by strong shallow anomalies. Synthetic experiments demonstrate the validity of the migration method for a variety of laterally heterogeneous models. The migrated images show considerable improvement over the CCP images in recovering the model features. Influences of several factors on the image quality of the poststack migration are further investigated, including interstation spacing, noise level of the data, velocity model used in migration, and earthquake distribution (incident direction of source fields). On the basis of the sampling theorem and previous statistic results, we discuss the relation of spatial resolution and signal-to-noise ratio of the migrated image with the frequency of the data, surface station spacing and number of receiver functions used in stacking. We show that both CCP stacking and poststack migration of receiver functions need to be designed in a target-oriented way for reliable and efficient imaging. Our results also suggest that careful consideration of earthquake source distribution is necessary in designing seismic experiments aimed at imaging steeply dipping structures.

**Citation:** Chen, L., L. Wen, and T. Zheng (2005), A wave equation migration method for receiver function imaging: 1. Theory, *J. Geophys. Res.*, 110, B11309, doi:10.1029/2005JB003665.

### 1. Introduction

[2] Many data processing techniques routinely applied in reflection seismology, such as the moveout correction and the common midpoint (CMP) stacking, have recently been modified to develop the common conversion point (CCP) stacking techniques to improve the signal-to-noise ratio for receiver function imaging using dense array data [e.g., Dueker and Sheehan, 1997; Li *et al.*, 1998; Owens *et al.*, 2000; Zhu, 2000; Ai *et al.*, 2003; Gilbert *et al.*, 2003]. Both the signal-to-noise ratio and the spatial resolution can be significantly improved by optimum CCP binning, moveout correction and subsequent stacking. However, in the same way that the CMP stacking method is based on a horizontal reflector model, the CCP stacking approach implicitly

assumes that the *P-SV* conversions occur at horizontal discontinuities. If significant lateral heterogeneities are present, structures cannot be correctly imaged by the CCP stacking of the receiver functions due to the diffraction or scattering artifacts produced by dipping and laterally discontinuous interfaces [Sheehan *et al.*, 2000; Abe and Brown, 2002]. Seismic migration techniques have been applied successfully in reflection seismology to eliminate such artifacts and typically produce significant improvements in reflection image quality [Stolt, 1978; Berkhouit, 1982; Claerbout, 1992; Gray and May, 1994]. Migration methods, however, work best in areas with dense data coverage. The low density and irregular distribution of the data prohibited wide applications of migration methods to processing teleseismic receiver functions in the past. Nowadays, the availability of a large number of broadband high-quality seismic stations provides the opportunity to apply advanced migration methods to more reliably image deep

structures using teleseismic data. Recently, several migration techniques have been introduced and adopted to image earth structure. For example, *Revenaugh* [1995] presented a Kirchhoff coda migration method for imaging crust and upper mantle structure using singly scattered energy within the coda of teleseismic  $P$  waves. *Shearer et al.* [1999] applied a backprojection migration approach to the  $S$ -to- $P$  scattered field in  $SS$  precursors, and *Sheehan et al.* [2000] experimented with a similar scheme using  $P$ -to- $S$  converted phases to study upper mantle discontinuities. *Ryberg and Weber* [2000] applied a poststack Kirchhoff depth migration method to synthetic data and demonstrate that the concept of migration of  $P$ -to- $S$  converted wave fields is theoretically sound. *Abe and Brown* [2002] discussed the applications of poststack and prestack Kirchhoff time migration techniques for teleseismic  $P$ -to- $S$  converted wave through synthetic testing. *Bostock and Rondenay* [1999], *Bostock et al.* [2001], *Rondenay et al.* [2001] and *Shragge et al.* [2001] suggested a migration method based on the inverse scattering theory that treats all  $P$  wave coda as energy caused by scatterers. Also, more recently, *Poppeliers and Pavlis* [2003a, 2003b] presented a plane wave migration technique for receiver function imaging using the  $\tau$ - $p$  transform. Their approach is comparable to a prestack migration method in reflection seismology.

[3] All of the receiver function migration methods developed to date are based on ray theory. Ray theory has been a basic tool to study various wave phenomena for some time [*Hubral*, 1977; *Aki and Richards*, 1980; *Sassolas et al.*, 1999; *Cervený*, 2001]. The ray methods, which rely on high-frequency asymptotic ray tracing, are known, however, to face problems in the presence of caustics, multiple arrivals, shadow zones, and even chaotic rays in complex environments [*Fei et al.*, 1996; *Audebert et al.*, 1997]. More accurate ray tracing that takes into account of multipathing and computes correct amplitudes of each arrival is computationally more expensive and more difficult to implement. Wave equation based methods can avoid these difficulties. Many of them have been employed in reflection data processing, when higher accuracy and resolution are required. Among them, the finite difference (FD) migration [*Claerbout and Doherty*, 1972; *Hale*, 1991] is the most flexible and accurate one, but it requires careful implementations to achieve numerical stability. Another group of wave equation based method is the frequency–wave number dual domain migration techniques, which simplify the evolution of the total wave field in a laterally homogeneous medium as the superposition of a set of simple and well-known solutions, the plane waves. The phase shift migration [*Gazdag*, 1978; *Stolt*, 1978] is the simplest one in this group, which has the attractive advantages such as exact implementation of the transversal differential operators in the wave equation, unconditional stability, and fast computational speed benefited from using the fast Fourier transform (FFT) to shuttle the wave fields between different domains. However, such a method uses a constant velocity of each depth interval and cannot handle lateral velocity variations. The split step Fourier or phase screen migration [*Stoffa et al.*, 1990; *Wu and Huang*, 1992], and the generalized screen migration [*Xie and Wu*, 1998; *De Hoop et al.*, 2000] were later developed to take into account the effects of lateral heterogeneity while retaining the advantages of the

phase shift migration. The screen-based methods have been recognized as an efficient and powerful imaging tool in reflection seismology [*Stoffa et al.*, 1990; *Xie and Wu*, 2001; *Jin et al.*, 2002]. In contrast to the plane waves employed in the screen methods, which have the highest directional resolution but occupy the whole space, the recently proposed beamlet migration method uses a set of spatially confined basic functions (beamlets) to decompose the wave field and construct the propagator in the decomposition domain (beamlet domain). Beamlets and propagators are localized in both space and direction, a very desirable feature for high-resolution imaging as well as reliable directivity-involved analysis [*Wu et al.*, 2000b; *Wu and Chen*, 2001; *Chen et al.*, 2005a]. However, such a method is computationally more expensive than the screen method, and it becomes not economical if directivity features are not particularly concerned.

[4] In the current work, we apply a poststack phase screen depth migration method to study the crustal and upper mantle discontinuities using time domain CCP stacked teleseismic receiver functions. This paper is the first of a two-part series. We introduce the theoretical aspects of our poststack migration method for receiver function imaging in section 2 and apply the proposed method to study several specially designed two-dimensional (2-D) models using synthetic receiver functions in section 3. We study in detail the effects on the poststack migrated images under different acquisition geometries, different noise levels, and with different migration velocity models in section 4. The second paper of this series focuses on the practical aspects of applying the wave equation migration technique to real data sets, and more detailed investigations of the imaged subducting slabs beneath Japan [*Chen et al.*, 2005b].

## 2. Poststack Phase Screen Migration of Receiver Functions

[5] Our poststack migration method consists of two basic procedures: CCP stacking and backward wave field extrapolation. CCP stacking is used to improve the signal-to-noise ratio of the data, similar to the CMP stacking of reflected data routinely used in reflection seismology. The backward wave field exploration is a migration process to project the convertors to their true positions using the CCP stacked record. In CCP stacking, receiver functions obtained for individual earthquakes are binned according to their sampling points, moveout corrected based on an one-dimensional (1-D) reference model, and subsequently stacked [e.g., *Dueker and Sheehan*, 1997; *Zhu*, 2000; *Ai et al.*, 2003]. The resultant CCP stacked gathers can be regarded as a good approximation to a zero-offset (zero source-receiver distance) data set, i.e., converted phases propagating vertically from the sampling points of the discontinuities to the surface directly above them. For complex subsurface structures, CCP stacking is known to produce artifacts in the images and migration is necessary to image the true position of convertors [*Ryberg and Weber*, 2000; *Poppeliers and Pavlis*, 2003a]. Our backward wave field extrapolation is a migration method similar to the exploding reflector model used in reflection seismology [*Claerbout*, 1985; *Sheriff and Geldart*, 1995]. In the exploding reflector model, each

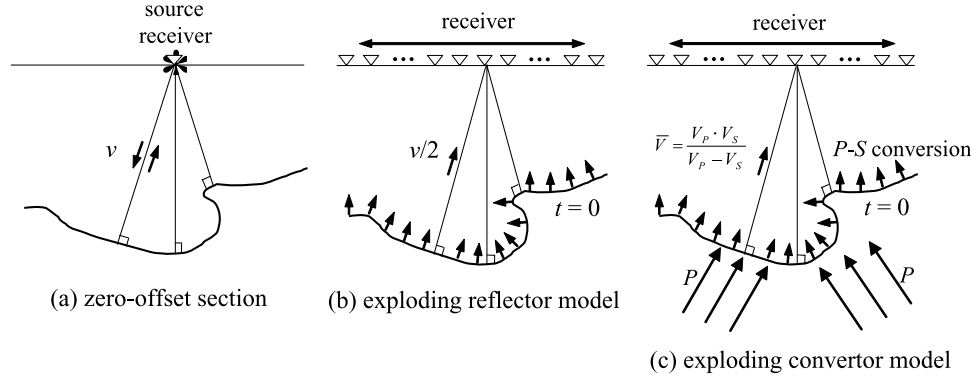


**Figure 1.** Schematic illustrations of (a) zero-offset section, (b) exploding reflector model employed in poststack migration in reflection seismology, and (c) the similar exploding convertor model that is based on our poststack depth migration for receiver functions.

reflecting interface is assumed to be a distributed source detonated at time  $t = 0$ , with its source density being proportional to the reflectivity at the interface; seismic waves are radiated upward at the half of the actual velocity (to account for two-way travel time) (Figures 1a and 1b). The record received at the surface of the Earth simulate the CMP stacked zero-offset (zero source-receiver distance) section. Migration reverses this process, i.e., backward propagates the zero-offset wave field observed at the surface to  $t = 0$ , and generates a depth-migrated image with all reflectors at their true positions. In our receiver function migration, the CCP stacked zero-offset receiver function gathers are treated as the surface wave field originated from all the subsurface convertors that are detonated simultaneously at  $t = 0$ , with its source intensity being proportional to the  $P$ - $SV$  transmission coefficient at the subsurface (Figure 1c). Such a model is called an exploding convertor model, which was first described and applied to receiver function imaging by Pavlis [2003]. The CCP stacked zero-offset receiver function gathers are backward propagated to the whole space and the migrated image of the convertors is constructed at  $t = 0$ . Our migration method is similar to that of Ryberg and Weber [2000], except that, while they used a ray-based Kirchhoff method to extrapolate the wave field, we employ a wave equation based technique.

[6] It should be also noted that, although we focus on developing theoretical formulations for imaging subsurface  $P$ -to- $S$  convertors in the following subsections, the basic ideal and principle can be directly applied to some other kinds of seismic signals, such as  $S$ -to- $P$  converted phases,  $P$ -to- $P$  and  $S$ -to- $S$  phases, and various surface-reflected multiples.

## 2.1. CCP Stacking

[7] The CCP stacking procedure consists of moveout correction, binning and stacking of the receiver functions. Each receiver function is moveout corrected to a zero pseudosource receiver distance (hypothetical antipode earthquake, or horizontal slowness  $p = 0$ ). The moveout correction is the time difference between the travel time of the  $P$ -to- $S$  conversion predicted based on an 1-D reference model and that of a zero pseudosource-receiver  $P$ -to- $S$  conversion, i.e.,

$$\Delta T_{PS}(p) = T_{PS}(p) - T_{PS}(0) \quad (1)$$

with the travel time of the  $P$ -to- $S$  conversion  $T_{PS}$  determined based on the assumption of a planar incident wave front in a flattened Earth [Gurrola et al., 1994; Dueker and Sheehan, 1997]

$$T_{PS}(p) = \int_D^0 \left( \sqrt{V_S^{-2}(z) - p^2} - \sqrt{V_P^{-2}(z) - p^2} \right) dz \quad (2)$$

where  $D$ ,  $V_P$  and  $V_S$  are the depth of the  $P$ -to- $S$  conversion, vertically varying  $P$  wave and  $S$  wave velocities, respectively. After the moveout correction, all traces are sorted into different conversion point bins with respect to each depth to achieve an optimum focusing effect. The resultant CCP stacked receiver function data set is approximately equivalent to the case of perpendicular  $P$  wave incidence.

## 2.2. Phase Screen Propagator

[8] Our migration scheme employs a wave equation based one-way operator decomposition and first-order screen approximation (phase screen propagator) to extrapolate the wave field from the time domain field at the surface (the CCP stacked receiver function gathers) to the space domain wave field at time  $t = 0$  (the image) in the frequency-wave number domain. In this paper, we limit our considerations to the 2-D ( $x, z$ ) case. The generalization to the 3-D case is straightforward. In frequency-space domain, the scalar wave equation can be written as

$$\left[ \frac{\partial^2}{\partial x^2} + \frac{\partial^2}{\partial z^2} + \frac{\omega^2}{v^2(x, z)} \right] u(x, z, \omega) = 0 \quad (3)$$

where  $\omega$  denotes the circular frequency,  $v(x, z)$  is the medium velocity, and  $u(x, z, \omega)$  represents the frequency-space domain wave field.

[9] On the basis of the perturbation theory, the medium velocity can be decomposed into a background velocity  $v_0(z)$  and a corresponding perturbation  $\delta v(x, z)$

$$v(x, z) = v_0(z) + \delta v(x, z) \quad (4)$$

Substituting equation (4) into (3) yields

$$\left( \frac{\partial^2}{\partial x^2} + \frac{\partial^2}{\partial z^2} + k_0^2 b^2 \right) u(x, z, \omega) = 0 \quad (5)$$

where  $k_0 = \omega/v_0(z)$  is the background wave number, and  $b(x, z) = v_0(z)/v(x, z)$  is the perturbation function. Equation (5) can be factored into two one-way wave equations, with one for forward propagation and the other for backward propagation. The equation governing the forward propagated wave field is

$$\frac{\partial u(x, z, \omega)}{\partial z} = i\sqrt{k_0^2 b^2 + \frac{\partial^2}{\partial x^2}} u(x, z, \omega) \quad (6)$$

The square root operator in the right-hand side of the equation has been expanded into perturbation series [De Hoop et al., 2000] or Padé expansions [Xie and Wu, 1998; Jin et al., 2002] under different considerations. The general expression of the wave equation becomes

$$\frac{\partial u(x, z, \omega)}{\partial z} = ik_0 b \left[ 1 + Q \left( k_0, b, \frac{\partial^2}{\partial x^2} \right) \right] u(x, z, \omega) \quad (7)$$

where  $Q$  represents the high-order expansion of the square root operator. The wave field can be expressed as a superposition of plane waves

$$u(x, z, \omega) = \int dk_x U(k_x, z, \omega) e^{ik_x x} \quad (8)$$

where  $U(k_x, z, \omega) e^{ik_x x}$  is a plane wave component with  $U(k_x, z, \omega)$  as its amplitude and  $k_x$  is the corresponding transverse wave number. Applying the Fourier transform over  $x$  to equation (7) yields

$$\frac{\partial U(k_x, z, \omega)}{\partial z} = i \left[ k_z - k_0 \left( FT_x \left[ \frac{\delta v}{v} \right] * \right) + Y(k_x, k_0, b) \right] U(k_x, z, \omega) \quad (9)$$

where  $k_z = \sqrt{k_0^2 - k_x^2}$  is the background vertical wave number.  $FT_x[\cdot]$  denotes the Fourier transform over  $x$ , asterisk represents the convolution in wave number domain, and  $Y$  is the Fourier transform of  $k_0 b Q$  over  $x$ . When the velocity perturbation is small ( $\delta v(x, z) \ll v(x, z)$ ) and the small angle approximation is valid ( $k_x^2 \ll k_0^2$ ),  $Y$  can be dropped from the above equation. The screen approximation can be made for the wave field that propagates through a thin slab between  $z_i$  and  $z_{i+1}$ . When the slab is thin enough, the variation of  $b(x, z)$  along  $z$  direction within the slab can be ignored and the wave field is simplified as [Stoffa et al., 1990; Xie and Wu, 1998]

$$U(k_x, z_{i+1}, \omega) = e^{ik_z(z_{i+1}-z_i)} \cdot FT_x \left[ \exp \left( -i \frac{\delta v(x, z_i)}{v(x, z_i)} k_0 (z_{i+1} - z_i) \right) u(x, z_i, \omega) \right] \quad (10)$$

With an additional inverse Fourier transform, the space domain field  $u(x, z_{i+1}, \omega)$  can be obtained. As shown in equation (10), the phase screen wave field extrapolation at each depth contains two steps: space domain phase correction  $\exp \{-i[\delta v(x, z_i)/v(x, z_i)]k_0(z_{i+1} - z_i)\}$  to account for lateral velocity perturbations and phase shift operation  $\exp[ik_z(z_{i+1} - z_i)]$  to account for wave propagation in the background medium. These two steps are carried out at

each depth to extrapolate the wave field from the surface to depths.

[10] A velocity model is required for the implementation of wave field extrapolation. Different from the reflection data, the travel time of a  $P$ -to- $S$  conversion in the receiver function is defined as the one-way delay time between the  $P$  and the converted  $S$  phase (equation (2)). In the moveout corrected CCP gathers, it becomes

$$T_{PS}(p=0) = \int_D^0 [V_S^{-1}(z) - V_P^{-1}(z)] dz = \int_D^0 \frac{dz}{\bar{V}(z)} \quad (11)$$

with

$$\bar{V}(z) = \frac{1}{V_S^{-1}(z) - V_P^{-1}(z)} = \frac{V_P(z)V_S(z)}{V_P(z) - V_S(z)} \quad (12)$$

as the equivalent wave velocity. By extending expression (12) to laterally varying velocity cases, we define the equivalent velocity for any arbitrary media

$$\bar{V}(x, z) = \frac{V_P(x, z)V_S(x, z)}{V_P(x, z) - V_S(x, z)} \quad (13)$$

$\bar{V}(x, z)$  is taken as the migration velocity in equation (10) for wave field extrapolation.

[11] Following the procedure in (10), the wave field at the surface is backward propagated to depth for each frequency. The final image of the poststack migration, that is, the wave field at  $t = 0$  based on the exploding convertor model, is constructed by superposing the migrated wave fields over the entire frequency range (inverse Fourier transform for  $t = 0$ )

$$I(x, z) = u(x, z, t = 0) = \sum_{\omega} u(x, z, \omega) \quad (14)$$

In the proposed wave equation poststack migration scheme, laterally velocity variations can be included in the migration velocity model, and therefore effects of lateral heterogeneities can be taken into account during the poststack migration procedure. The phase screen propagator has been proven to be accurate enough to handle smoothly varying lateral velocities, and even for abrupt velocity discontinuities with velocity perturbations as large as 40% [Stoffa et al., 1990]. For more complicated situations or larger velocity perturbations, more accurate wave field propagators, such as the generalized screen propagator [Xie and Wu, 1998; De Hoop et al., 2000] or beamlet propagator [Wu et al., 2000b; Wu and Chen, 2001], or prestack migration may be needed to improve the image quality. Furthermore, in the cases where the 2-D assumption becomes invalid, three-dimensional (3-D) migration techniques have to be applied to correctly account for the wave field propagation effects in complex environments. With the migration framework introduced above, accurate propagators for both 2-D and 3-D wave fields can be easily incorporated into the migration process to replace the phase screen propagator used in this study. Corresponding prestack migration schemes can also be readily established

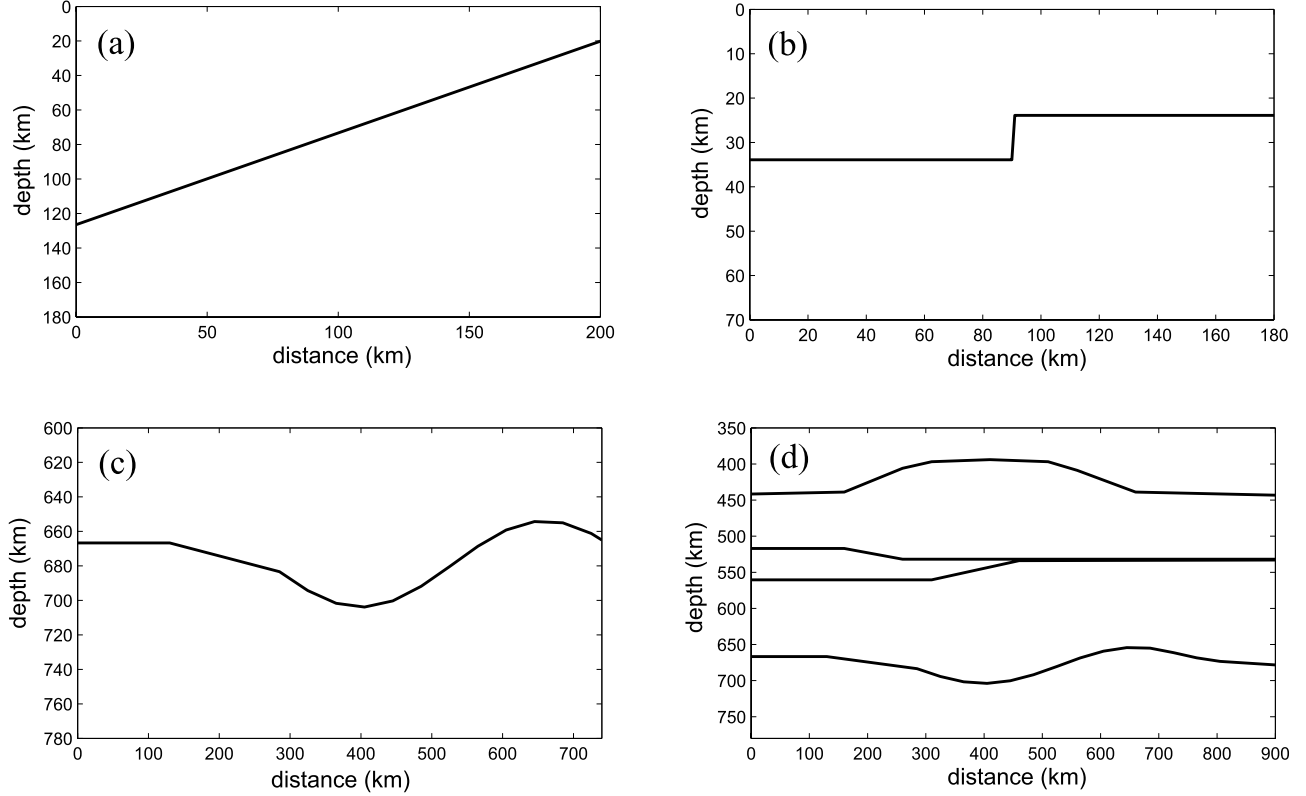


**Figure 2.** The 2-D models used for simulations.

on the basis of the principle and procedure similar to their reflection seismology version.

[12] It should be noted that the proposed phase screen propagator migration method is a Fourier transform-based method that requires uniform sampling of data in both time and space. Seismic data generally have uniform time sampling but highly irregular spatial distribution. For post-stack migration, regular spatial sampling can be achieved by CCP stacking within regularly spaced bins; while for pre-stack migration, some regulation techniques are needed to attain evenly distributed data in space, such as the pseudostation stacking technique proposed by *Neal and Pavlis* [1999] and *Poppeliers and Pavlis* [2003a, 2003b]. On the other hand, with the implementation of wave field extrapolation in frequency domain, it becomes simple and efficient to use the proposed migration method to construct images with different frequency contents. This can be done by directly summing up the migrated wave fields of expected frequencies. Compared with stacking-based or time domain receiver function imaging techniques, in which filtering is always required to best extract information in a certain frequency range, the frequency domain implementation makes the proposed wave equation migration technique an efficient tool to study frequency- (or scale-) dependent features of subsurface structures.

### 3. Synthetic Experiments

[13] In order to test the validity and effectiveness of the proposed poststack phase screen depth migration scheme, a number of synthetic experiments are performed. We consider lateral heterogeneous structures in the receiver side

from the surface up to 750-km depth. For each model, we calculate synthetic seismograms based on the model, construct receiver functions from the synthetic seismograms, perform CCP stacking and phase screen propagator migration, and compare the migrated images with the original model. Synthetic seismograms are calculated based on a 2-D  $P$ - $SV$  hybrid method [*Wen and Helmberger*, 1998], in which the generalized ray theory (GRT) solutions are used to construct the wave field in the homogeneous medium, while a staggered grid FD technique is applied to the region where heterogeneous structures are involved. In this study, the direct  $P$  wave is constructed from the GRT solutions for the Preliminary Earth Reference Model (PREM) [*Dziewonski and Anderson*, 1981], and those solutions are interfaced with the FD calculation at the bottom and left boundaries or right boundaries (depending on the incident direction) of the heterogeneous FD region. From the output synthetics of the FD calculation at the surface, receiver functions are constructed based on the frequency domain deconvolution method [*Ammon*, 1991]. A low-pass Gaussian filter width of 2 (corresponding to  $\sim 1$  Hz) is used for receiver function calculation.

[14] We present results for four 2-D models in this study. The first model contains a discontinuity dipping from  $\sim 20$  km depth to 140 km with a dip of about  $30^\circ$  (Figure 2a). Dipping structure is often regarded as a characteristic for a subduction zone area [*Bostock et al.*, 2002; *Ferris et al.*, 2003]. The second model is characterized by an offset of the Moho discontinuity (Figure 2b). Such an offset may take place across major faults, such as the Tancheng-Lujiang fault in eastern China [*Wang et al.*, 2000] or the San Andreas fault in the western United States [*Henstock et al.*, 1997; *Zhu*, 2000].

The third model consists of a curved discontinuity around 660-km depth (Figure 2c). Such an undulation of the 660-km discontinuity may exist when thermal anomalies are present, such as near a subduction slab [e.g., *Shearer et al.*, 1999]. The fourth model is more complex, containing undulating 410-km and 660-km discontinuities, and a partially doubled 520-km discontinuity (Figure 2d). The anticorrelated topography of the 410- and 660-km discontinuity may represent a cold subducting slab entering the upper mantle transition zone if regular Clapeyron slopes of the olivine component of mantle composition are considered for both discontinuities [*Helffrich*, 2000; *Lebedev et al.*, 2002]. Synthetic seismograms from earthquake simulation with epicentral distances ranging from  $30^\circ$  to  $90^\circ$  are generated and the corresponding receiver functions are calculated. Figure 3 compares the receiver functions of the 2-D models with those of the PREM. Distinct lateral variations in receiver functions are observed for all these inhomogeneous cases (Figure 3).

[15] For each 2-D model, the delay times of the  $P$ -to- $S$  converted phases relative to the direct  $P$  wave and the piercing points of the conversions at the discontinuities are calculated based on a simplified 1-D velocity model derived by laterally averaging the velocities of the true model. During the CCP stacking process for the receiver functions, bins are designed to be equally spaced but the width of bins is allowed to vary along the stacking profile according to the data coverage. The bin width is increased from a minimum width until the specified minimum number of receiver functions in each bin is met or a maximum allowable bin width is reached. For the synthetic tests in this study, the minimum and maximum bin widths are depth-dependent, for example, 10 and 100 km for the upper 200 and 40 km and 240 km for the 350–800 km depth range, respectively. The minimum receiver function number in each bin is kept to be 10. It is particularly desirable to use variable bin widths in the stacking in the areas with highly uneven sampling coverage. It enhances small-scale features in the areas with dense data sampling and constructs continuous structural image in areas with less data sampling. The separations between the centers of the bins are designed to be 2 km and 5 km for the structures above and below 200 km, respectively, to avoid loss of spatial resolution in imaging results. After the CCP stacking, the stacked receiver functions are input as the initial wave field to the poststack phase screen depth migration program and the final image is derived from the migrated wave field based on equation (14).

[16] The images by poststack migration for the four 2-D models along those obtained by the CCP stacking [*Zhu*, 2000] are shown in Figure 4. These two sets of images are obtained with an interstation spacing of 10 km and a same average 1-D velocity model. This allows us to directly compare the two groups of images and to see their systematic differences. The CCP depth images have similar appearance as those of the unmigrated time domain CCP receiver functions (not shown here), since very similar stacking principles are adopted in their construction processes despite the different domains the stacking is implemented. The assumption of a horizontal and planar structure adopted in the CCP stacking leads to either distortion of the shape of the discontinuities, such as the shallowed dipping

structure (Figure 4a) and the deformed 660-km discontinuities (Figure 4c and 4d), or defocusing of the diffracted energies, as manifested by the ambiguous location of the Moho step (Figure 4b) and the long tails around the bottom turning point of the 660-km discontinuities (Figure 4c and 4d). In contrast, the migration scheme significantly reduces the unwanted stacking effects and properly accounts for the propagation effects of lateral heterogeneities during the wave equation based wave field extrapolation procedure (Figures 4e, 4f, 4g, and 4h). The migration processes substantially suppress the diffraction artifacts and multiple noise, and result in correctly imaged dipping and curved discontinuities. The improved spatial resolution for the Moho step is evident even with the 1-D migration velocities (Figure 4f). Comparison of the migrated images with the CCP depth images demonstrate the great advantages of the proposed receiver function migration scheme in improving the image quality for both crustal and upper mantle structures.

#### 4. Factors Influencing the Migrated Images

[17] Receiver function migrated images are influenced by various factors, including surface acquisition system that involves both station location and source (earthquake) distribution, signal-to-noise ratio of the data, propagation effects of overlying structures, and velocity model used in imaging, etc. Next, we investigate in detail the sensitivity of the migrated images to each of these factors.

##### 4.1. Interstation Spacing

[18] Surface acquisition geometry determines the spatial resolution of the migrated images. The above synthetic experiments are performed using a uniform interstation spacing of 10 km. We study effects on the migrated images of larger uniform interstation spacings and nonuniform data distribution. Figure 5 shows the poststack migrated images for the models of dipping structure and curved 660-km discontinuity with uniform interstation spacings (thus uniform data distribution) of 10, 50, and 100 km, respectively. Randomly selected subset of the data with an average spacing of 50 km is also considered here to simulate the nonuniform data coverage. The true 2-D velocity models are used in the migration procedures.

[19] A 10-km interstation spacing is sufficient for imaging both the shallow and the deep discontinuities (Figures 5a and 5e). A 50-km interstation spacing is apparently too large to image the shallow structure coherently (Figure 5b), but it produces a rather good image for the undulating 660-km discontinuity (Figure 5f). The image quality of the undulating 660-km discontinuity is even comparable with that in the 10-km spacing case (Figure 5e). When the station spacing reaches 100 km, reliable images cannot be derived for both input models (Figures 5c and 5g). In the situation of random station spacing, uneven data coverage leads to variable bin sizes in the CCP stacking process and hence results in different spatial resolution in different parts of the migrated image. This is particularly evident in the image of the shallow dipping structure (Figure 5d). Note that the image has a higher spatial resolution in the lower part and a poorer quality in the upper part compared with the image with a regular station spacing (Figure 5b). The effect of the uneven data distribution is not so important for the 660-km discontinuity (Figure 5h),

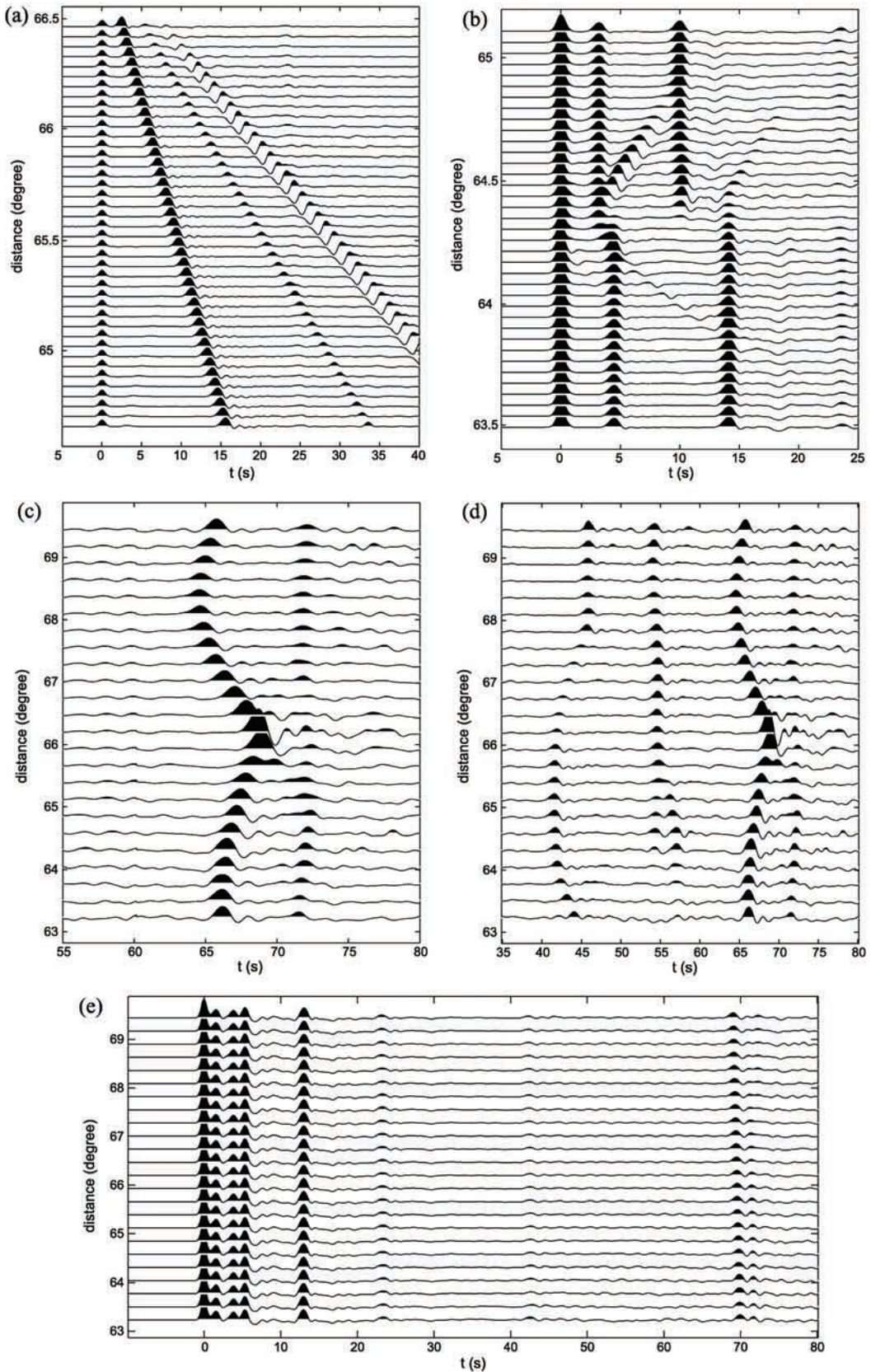


**Figure 3.** Receiver functions examples (a–d) for the study models shown in Figures 2a–2d and (e) for PREM. For each study model, only part of the receiver functions in the time window containing the phases from the heterogeneous structures are shown.

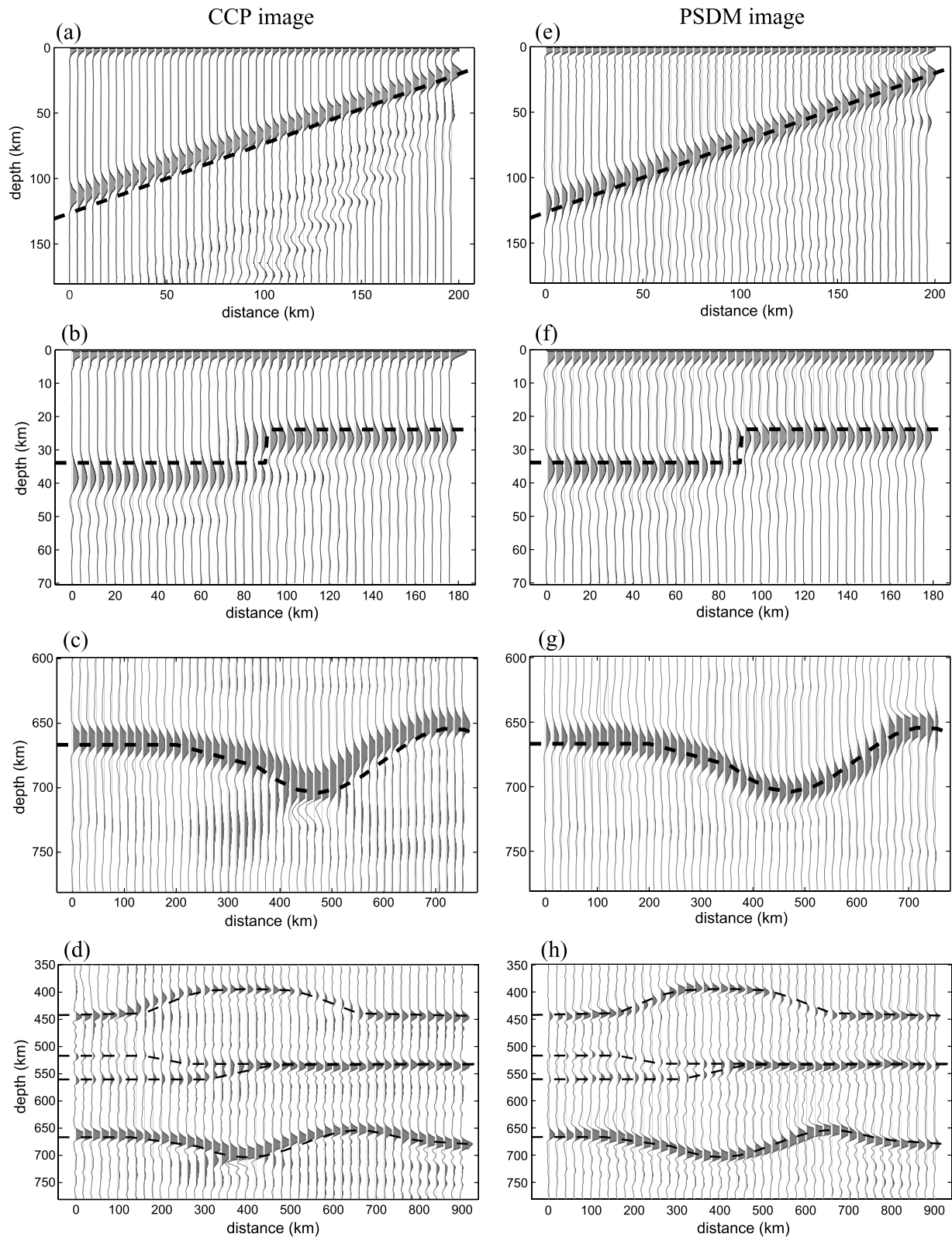


**Figure 4.** (e–h) Poststack migrated images along with (a–d) CCP depth images for the study models. All images are constructed using receiver functions 10 km apart at the surface from eight earthquakes of left-side incidence. Thick dashed lines (here and in Figures 5–8) mark the model discontinuities.

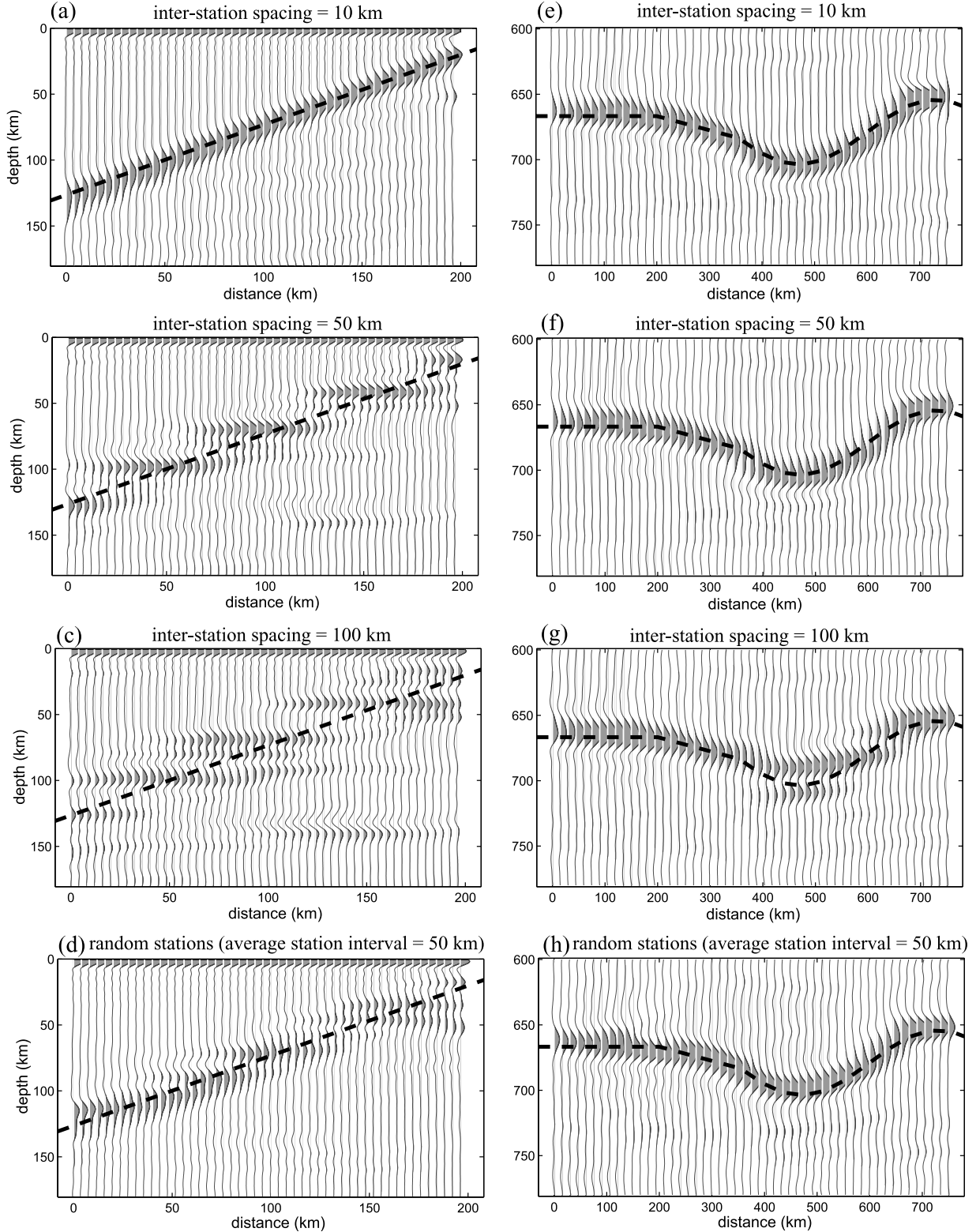


**Figure 5.** Migrated images with various interstation spacing: (a, e) 10 km, (b, f) 50 km, (c, g) 100 km, and (d, h) average 50 km with randomly selected data for the models of the dipping discontinuity (Figures 5a–5d) and the curved 660-km discontinuity (Figures 5e–5h).

partially because the 50-km interstation spacing is sufficient for clearly imaging such a deeper structure. The smooth varying feature of the 660-km discontinuity also makes it less sensitive to the data density.

[20] The above migration experiments with various interstation spacings show that the proposed poststack migration scheme works better with spatially denser data. Coarse sampling may result in considerable deterioration of the

migrated image, which becomes particularly serious for the shallow structures. This observation is consistent with the spatial resolution constraint of seismic images that has been studied extensively for reflection data migration [Beylkin *et al.*, 1985; Safar, 1985; Bleistein, 1987; Vermeer, 1998; Chen and Schuster, 1999]. The general consensus is that the horizontal and vertical resolution is a function of spatial sampling, station aperture, and depth of the target structure. Safar [1985] shows that the lateral resolution is proportional to the depth of the targeted structure and is inversely proportional to the surface acquisition aperture, and a large spatial sampling interval could cause generation of imaging noise. Similar conclusions are also obtained with different criteria and in different theoretical aspects [Vermeer, 1998; Chen and Schuster, 1999].

[21] Spatial sampling, data frequency and targeted depth of the structure are related in affecting the resolution of the poststack migration results. The sampling theorem states that signals should be sampled at least twice per wavelength. The highest frequency of interest  $f_{\max}$  and the maximum horizontal slowness  $p_{\max}$  determine the shortest apparent wavelength and thus the maximum permissible subsurface spacing. At a particular depth, the maximum spatial interval  $\Delta x_{\max}$  of receiver functions is constrained as

$$\Delta x_{\max} \leq \frac{(\lambda_a)_{\min}}{2} = \frac{\lambda_{\min}}{2 \sin \alpha_{\max}} = \frac{V_{S\min}}{f_{\max} 2 \sin \alpha_{\max}} = \frac{1}{2 f_{\max} p_{\max}} \quad (15)$$

where  $\lambda_{\min}$  is the minimum wavelength,  $(\lambda_a)_{\min}$  is the minimum apparent wavelength at that depth, and  $\alpha_{\max}$  is the maximum incident angle of the seismic wave.  $V_{S\min}$  is the minimum  $S$  wave velocity, and we have  $\sin \alpha_{\max} / V_{S\min} = p_{\max}$ . The maximum horizontal slowness  $p_{\max}$  for the receiver function imaging is about 0.08 s/km (corresponding to the  $P$ -to- $S$  converted wave at a minimum epicentral distance of 30°). From equation (15), we can infer that the maximum spatial interval of receiver functions for a targeted depth is inversely proportional to the highest frequency of interest

$$\Delta x_{\max} \propto 1/f_{\max} \quad (16)$$

For a maximum frequency  $f_{\max} = 1$  Hz, the maximum interval of receiver functions  $\Delta x_{\max}$  is about 6 km, independent of the depth of the target discontinuity. In most of the receiver function studies, high-frequency contents of the receiver functions are usually filtered out to eliminate noise. The deeper the structure to be imaged, the lower the cutoff frequency is usually adopted in filtering. Therefore the required spatial sampling spacing actually increases with depth. A large station spacing, while producing deteriorated images for the shallow structures, can still result in reasonably good images for deeper structures (see the example in Figure 5).

#### 4.2. Noise Level of the Data

[22] In practical situations, noise is unavoidably embedded in the real data set and always tends to deteriorate the image quality. To test the capability of our migration method in noise suppression, we add random noises of different levels to the synthetic seismograms used above, and stack and migrate the resultant receiver functions. Here we define the noise level as the maximum amplitude ratio of

the noise to the noise-free seismogram. Figure 6 shows the resultant images without noise, with noise level of 50%, 100% and 200%, respectively, for the two models studied in Figure 5. Comparisons between Figures 6a and 6b and between Figures 6e and 6f show that small noise (50% noise level) in the data can be effectively suppressed and little effect can be traced in the migration results for both the shallow dipping structure and the undulating 660-km discontinuity. Synthetic experiments indicate that, for the station spacing and source distribution specified in the experiments, our migration method can effectively recover the model features with a noise level as large as 100%, although not all the noise is completely suppressed (Figures 6c and 6g). High levels of noise could significantly deteriorate the imaging quality, for example, receiver functions with a noise level of 200% are unable to recover the model features for both the dipping and the 660-km discontinuity models (Figures 6d and 6h).

[23] All the imaging techniques rely on record summation (stacking) for noise reduction. The signal-to-noise enhancement is qualitatively proportional to the number of receiver functions used for the stacking. Morozov and Dueker [2003] proposed, from a statistics point of view and based on simulations of white noise, that the signal-to-noise ratio in the resultant image is proportional to the square root of the number of receiver functions used in stacking. Since the proposed wave equation poststack migration presents superior ability in noise suppression than the CCP depth imaging (see examples in Figure 4) and real seismic data have strongly colored noise rather than only white noise, the method proposed in the Morozov and Dueker's study may only be used to provide an order of magnitude estimate for the signal-to-noise ratio in the migrated images.

[24] A balance, however, should be made between the signal-to-noise ratio enhancement (number of receiver functions in each bin) and the spatial resolution (bin size) in receiver function migration. For a given data set, a larger bin size would lead to a larger number of receiver functions that can be stacked in the CCP stacking, and thus a more noise-suppressed stacked receiver function; on the other hand, a larger bin size means that the observations are more laterally smoothed and the spatial resolution of the images decreases for the target discontinuities. Within tolerable signal-to-noise ratios, a small bin size is preferred when detailed structural features are of particular interest.

#### 4.3. Shallow Structure and Velocity Models

[25] One of the advantages of our proposed phase screen propagator is that lateral variations of seismic velocity can be appropriately taken into account in the migration procedure. At present, horizontal layered models are employed in most receiver function imaging techniques [Dueker and Sheehan, 1997; Zhu, 2000; Ai *et al.*, 2003; Li and Yuan, 2003; Gilbert *et al.*, 2003]. When significant shallow velocity variations are present, the 1-D approximation or incorrect velocity models may cause defocusing of the diffracted/scattered energies and hence reduce the image quality of the target discontinuity [Ryberg and Weber, 2000]. The ability to incorporate 2-D velocities into the migration procedure is essential in constructing high-quality images for subsurface discontinuities that are overlain by strong lateral structural anomalies.

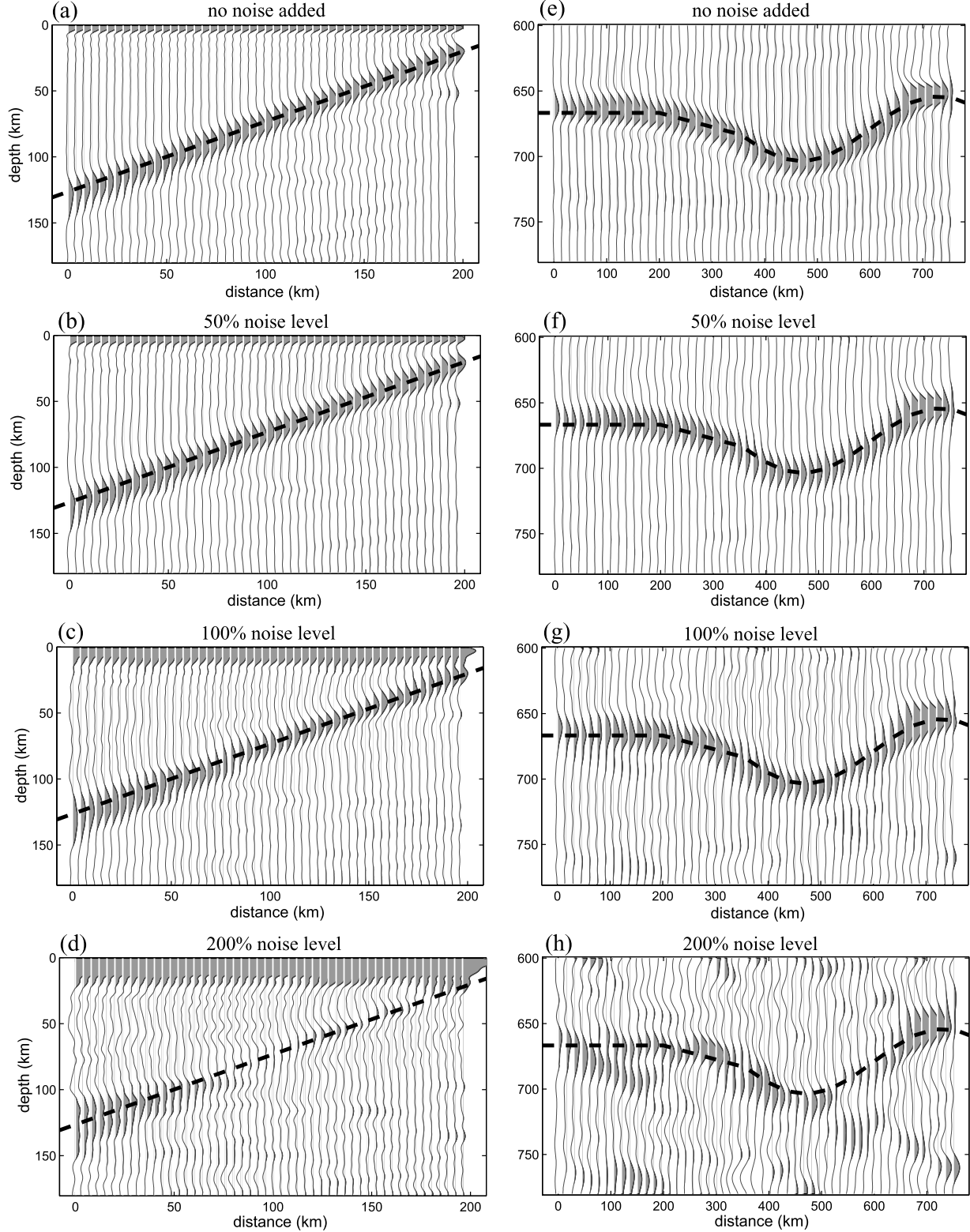


**Figure 6.** Migrated images with different levels of noise added in the synthetics: (a, e) no noise, (b, f) 50%, (c, g) 100%, and (d, h) 200% for the models of the dipping discontinuity (Figures 6a–6d) and the curved 660-km discontinuity (Figures 6e–6h).

[26] To investigate the effect of overlying lateral heterogeneity on the poststack migrated images, we test two models of different vertical scales (Figures 7a and 7e). The first model is constructed by superposing a laterally

varying low-velocity layer (basin) to a homogeneous one-layer crust. The second model, in contrast, consists of a significantly distorted crust overlain by a thicker basin layer and three horizontal discontinuities at 210-, 410-, and 670-km

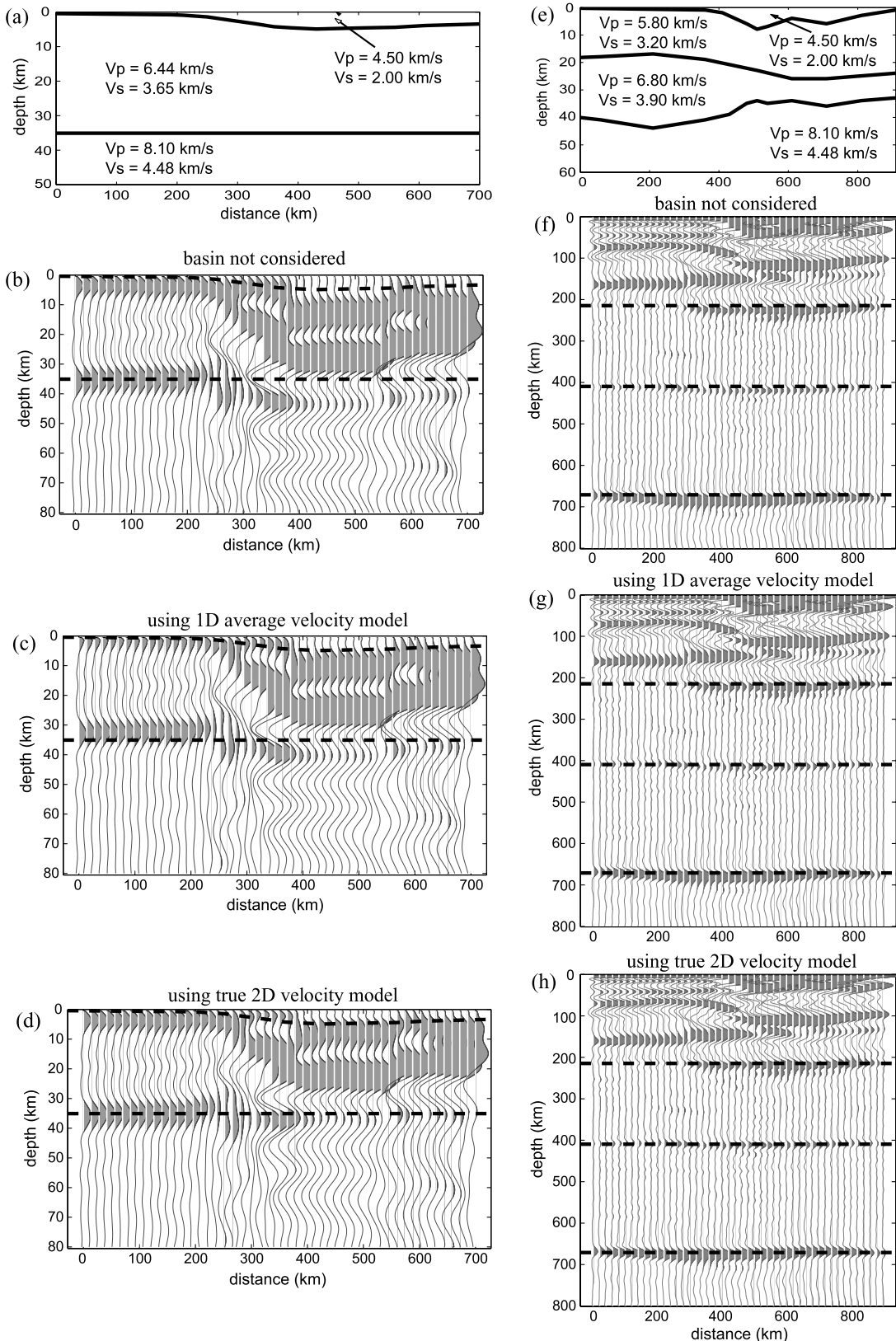


**Figure 7.** Two models containing shallow structural anomalies (Figures 7a and 7e) and migrated images (Figures 7b–7d and 7f–7h) using different migration velocity models: (b, f) 1-D model without the low-velocity basin; (c, g) 1-D laterally averaged velocity model; and (d, h) true 2-D velocity model.

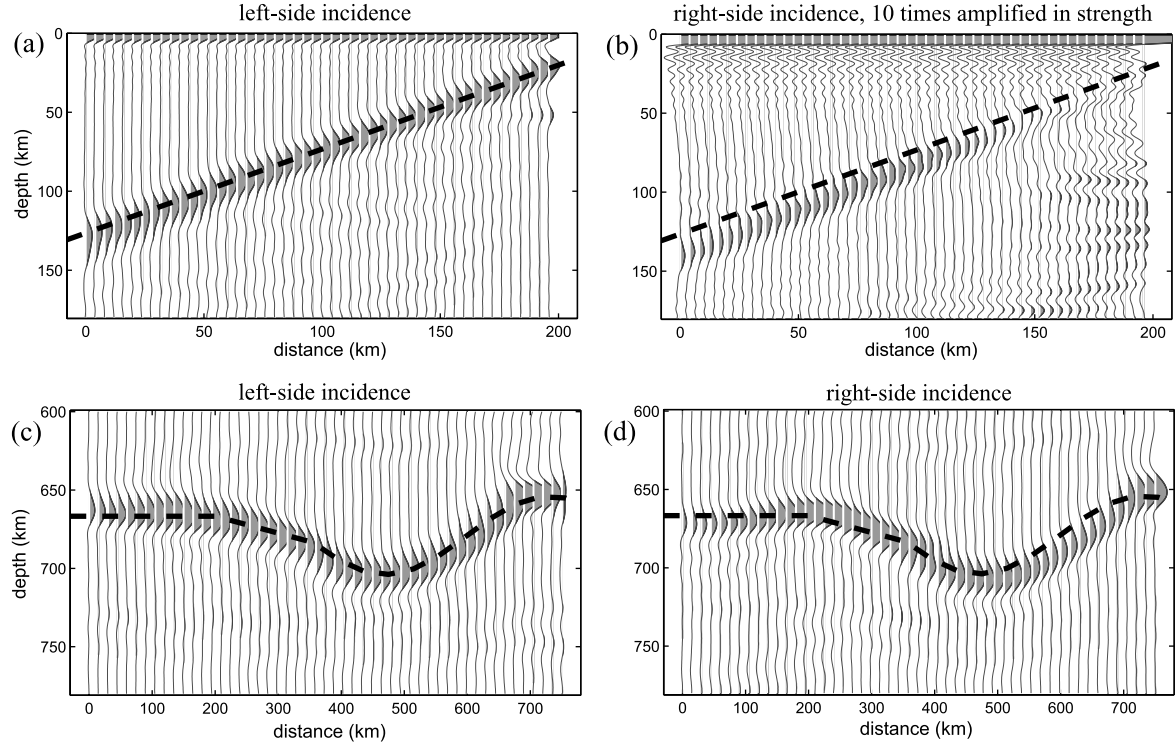


**Figure 8.** Migrated images of synthetics with different earthquake distributions (incident directions: (a, c) left-side incidence and (b, d) right-side incident) for the models of the dipping discontinuity (Figures 8a and 8b) and the curved 660-km discontinuity (Figures 8c and 8d). The image strength in Figure 8b is 10 times amplified.

depths, respectively. Different velocity models, including the 1-D model without considering the low-velocity basin, the 1-D model with laterally averaged velocity, and the correct 2-D model, are used in the migration process to derive the structural images (Figures 7b–7d and 7f–7h). The strong lateral variation of the uppermost low-velocity basin causes both mislocation and striking deformation of the Moho in the 1-D model-based images of the crust model (Figures 7b and 7c). With the true 2-D velocity model employed in migration, the image quality is remarkably improved with the Moho discontinuity horizontally aligned and migrated to its true depth (Figure 7d). Of course, in practice, the accuracy of the imaged depth depends on the accuracy of the 2-D velocity model used in migration. The quality of the migrated image could also be severely contaminated by the strong multiple reverberations of the basin, regardless of the migration velocity model used. For example, for the second model, the existence of shallow structures results in heavy interference of the internal multiples with the expected  $P$ -to- $S$  phases, making it difficult to clearly image the crustal structure (Figures 7f–7h). Such interference does not exist for deep converted phases. While the three deep discontinuities appear slightly deepened when the shallow low-velocity anomaly is not appropriately accounted for (Figures 7f and 7g), they are correctly imaged when the correct 2-D velocity model is adopted in migration (Figure 7h).

#### 4.4. Earthquake Distribution

[27] The migrated images would also depend on the direction the seismic waves sample the subsurface structures. The above images are obtained from receiver func-

tions of eight left-side incident earthquakes with epicenter distances uniformly distributed from  $30^\circ$  to  $90^\circ$ . We investigate the case using same number of earthquakes incident from the right side of the models, and compare the migrated images with those obtained from the left-side incident simulations (Figure 8). Some distinct discrepancies are observed, especially for the shallow dipping discontinuity model. The  $P$  waves incident from the right side strike the dipping discontinuity at nearly normal incident angles, therefore produce very small  $P$ -to- $S$  conversions and result in a significantly weakened image (Figure 8b). Note that the energy appearing in the images obtained based on the synthetics of the right-side incidence is at least 1 order of magnitude lower than that with left-side incidence (Figure 8a). On the other hand, the horizontal structure assumption adopted in CCP stacking is never valid for such a steeply dipping structure. The inappropriate moveout correction inevitably lead to considerable travel time errors in the stacked receiver functions, and finally cause the mismatch between the imaged discontinuities with the true model even with the correct velocity model adopted in the migration processes. The situation is apparently more serious for the right part of the deep 660-km discontinuity (Figure 8d) where the structure displays a similar left-down dipping direction as the shallow dipping structure. However, the image strength is only slightly reduced due to the smaller dipping angle ( $\sim 15^\circ$ ) and the more oblique incidence of  $P$  waves at larger depth.

[28] The substantial impacts of earthquake distribution on the image quality of subsurface structures have also been

documented in other receiver function studies for both synthetic models [Ryberg and Weber, 2000] and subduction zone areas of the real Earth [Ferris et al., 2003]. Either a complete coverage or favorable incident directions of the data is necessary for correctly imaging the target discontinuities of large dips. Nevertheless, nonideal earthquake distributions may still produce reasonable migration results in case of dense station spacing and weak directivity feature of the structures involved, as exemplified by the left part of the 660-km discontinuity that is well imaged by both the left- and right-side earthquake distributions (Figures 8c and 8d).

[29] In addition to the  $P$ -to- $S$  converted phase, other seismic phases upon different incident directions may be used to mitigate the effect of nonideal earthquake distribution. For example, backward reflected multiples from surface, complementary to forward scattered part of wave fields, have been proven to be useful in recovering structural feature [Shragge et al., 2001; Rondenay et al., 2001] and in distinguishing effective signals from noise-induced artifacts [Chen et al., 2005b].

## 5. Conclusions

[30] We present a wave equation based poststack migration scheme that utilizes a frequency–wave number domain one-way phase screen propagator to extrapolate the receiver function wave field in depth to image the Earth's internal structure. The phase screen propagator is capable of handling laterally varying velocities with perturbations large enough to meet the requirement for imaging most of the crustal and upper mantle structures. The synthetic experiments demonstrate that the proposed wave equation poststack depth migration method can be used to image crustal and upper mantle discontinuities. For laterally inhomogeneous structures, the migration procedure significantly improves the quality of the images over those obtained by the CCP stacking method. Detailed analyses show that the frequency content of the data, the surface station spacing and the number of receiver functions used in stacking are mutually related, and are important in determining the spatial resolution and the signal-to-noise ratio of the migrated receiver function image. Even with densely distributed data, the spatial resolution of receiver function images will still be subject to the constraint of the signal frequencies that decreases with the depth of the structure considered. Therefore both the CCP stacking and poststack migration should be designed in a target-oriented way to achieve subsurface structural imaging both reliably and economically. Our migration scheme can be extended straightforward to three-dimensional (3-D) receiver function imaging by simply replacing the 2-D wave field propagator with that for 3-D wave fields.

[31] **Acknowledgments.** We are grateful to Rushan Wu and Xiaobi Xie for thoughtful discussions on wave field extrapolation, Gary Pavlis, an anonymous reviewer, and Associate Editor for thoughtful reviews. This work was supported by the National Science Foundation of China (grant 40374015), the Chinese Academy of Sciences, and an NSF grant 0309859.

## References

- Abe, S., and L. D. Brown (2002), CCP stacking and migration of teleseismic P-SV converted wave, 72nd Annual International Meeting, Soc. Explor. Geophys., Salt Lake City, Utah.
- Ai, Y., T. Zheng, W. Xu, Y. He, and D. Dong (2003), A complex 660 km discontinuity beneath northeast China, *Earth Planet. Sci. Lett.*, **212**, 63–71.
- Aki, K., and P. G. Richards (1980), *Quantitative Seismology: Theory and Methods*, vol. I, W. H. Freeman, New York.
- Ammon, C. J. (1991), The isolation of receiver effects from teleseismic  $P$  waveforms, *Bull. Seismol. Soc. Am.*, **81**, 2504–2510.
- Audebert, F., D. Nichols, T. Rekdal, B. Biondo, D. E. Lumley, and H. Urdaneta (1997), Imaging complex geologic structure with single-arrival Kirchhoff prestack depth migration, *Geophysics*, **62**, 1533–1543.
- Berkhout, A. J. (1982), *Seismic Migration: Imaging of Acoustic Energy by Wave Field Extrapolation*, 2nd rev. and enlarged ed., Elsevier, New York.
- Beylkin, G., M. Oristaglio, and D. Miller (1985), Spatial resolution of migration algorithm, in *14th International Symposium on Acoustical Imaging, Proceedings*, edited by A. J. Berkhout, J. Ridder, and L. F. van der Waals, pp. 155–167, Springer, New York.
- Bleistein, N. (1987), On the imaging of reflectors in the Earth, *Geophysics*, **52**, 931–942.
- Bostock, M., and S. Rondenay (1999), Migration of scattered teleseismic body waves, *Geophys. J. Int.*, **137**, 732–746.
- Bostock, M., S. Rondenay, and J. Shragge (2001), Multiparameter two-dimensional inversion of scattered teleseismic body waves: 1. Theory for oblique incidence, *J. Geophys. Res.*, **106**, 30,785–30,796.
- Bostock, M., R. D. Hyndman, S. Rondenay, and S. M. Peacock (2002), An inverted continental Moho and serpentinization of the forearc mantle, *Nature*, **417**, 536–538.
- Cervený, V. (2001), *Seismic Ray Theory*, Cambridge Univ. Press, New York.
- Chen, J., and G. T. Schuster (1999), Resolution limits of migrated images, *Geophysics*, **64**, 1046–1053.
- Chen, L., R. S. Wu, and Y. Chen (2005a), Target-oriented beamlet migration based on Gabor-Daubchies frame decomposition, *Geophysics*, in press.
- Chen, L., L. Wen, and T. Zheng (2005b), A wave equation migration method for receiver function imaging: 2. Application to the Japan subduction zone, *J. Geophys. Res.*, **110**, B11310, doi:10.1029/2005JB003666.
- Claerbout, J. F. (1985), *Imaging the Earth's Interior*, Blackwell Sci., Malden, Mass.
- Claerbout, J. F. (1992), *Earth Soundings Analysis: Processing Versus Inversion*, Blackwell Sci., Malden, Mass.
- Claerbout, J. F., and S. M. Doherty (1972), Downward continuation of moveout-corrected seismograms, *Geophysics*, **37**, 741–768.
- De Hoop, M., J. Rousseau, and R. S. Wu (2000), Generalization of the phase-screen approximation for the scattering of acoustic waves, *Wave Motion*, **31**, 43–70.
- Dueker, K. G., and A. F. Sheehan (1997), Mantle discontinuity structure from midpoint stacks of converted  $P$  to  $S$  waves across the Yellowstone hotspot track, *J. Geophys. Res.*, **102**, 8313–8327.
- Dziewonski, A., and D. L. Anderson (1981), Preliminary reference Earth model, *Phys. Earth Planet. Inter.*, **25**, 297–356.
- Fei, T., M. C. Fehler, and S. T. Heldebrand (1996), Depth migration artifacts associated with first-arrival travel-time, paper presented at 66th Annual International Meeting, Soc. of Expl. Geophys., Denver, Colo.
- Ferris, A., G. A. Abers, D. H. Christensen, and E. Veenstra (2003), High resolution image of the subducted Pacific (?) plate beneath central Alaska, 50–150 km depth, *Earth Planet. Sci. Lett.*, **214**, 575–588.
- Gazdag, J. (1978), Wave equation migration with the phase-shift method, *Geophysics*, **43**, 1342–1351.
- Gilbert, H. J., A. F. Sheehan, K. G. Dueker, and P. Molnar (2003), Receiver functions in the western United States, with implications for upper mantle structure and dynamics, *J. Geophys. Res.*, **108(B5)**, 2229, doi:10.1029/2001JB001194.
- Gray, S. H., and W. P. May (1994), Kirchhoff migration using eikonal equation traveltimes, *Geophysics*, **59**, 810–817.
- Gurrola, H., J. B. Minster, and T. Owens (1994), The use of velocity spectrum for stacking receiver functions and imaging upper mantle discontinuities, *Geophys. J. Int.*, **117**, 427–440.
- Hale, D. (1991), 3-D depth migration by McClellan transformations, *Geophysics*, **56**, 1778–1785.
- Helffrich, G. (2000), Topography of the transition zone seismic discontinuity, *Rev. Geophys.*, **38**, 141–158.
- Henstock, T. J., A. Levander, and J. A. Hole (1997), Deformation in the lower crust of the San Andreas Fault System in northern California, *Science*, **278**, 650–653.
- Hubral, P. (1977), Time migration: Some ray theoretical aspects, *Geophys. Prospect.*, **25**, 738–745.
- Jin, S., C. C. Mosher, and R. S. Wu (2002), Offset-domain pseudoscreen prestack depth migration, *Geophysics*, **67**, 1895–1902.
- Lebedev, S., S. Chevrot, and R. D. van der Hilst (2002), Seismic evidence for olivine phase changes at the 410- and 660-kilometer discontinuities, *Science*, **296**, 1300–1302.

- Li, A., K. M. Fischer, M. E. Wysession, and T. J. Clarke (1998), Mantle discontinuities and temperature under the North American continental keel, *Nature*, **395**, 160–163.
- Li, X., and X. Yuan (2003), Receiver functions in northeast China: Implications or slab penetration into the lower mantle in northwest Pacific subduction zone, *Earth Planet. Sci. Lett.*, **216**, 679–691.
- Morozov, I. B., and K. G. Dueker (2003), Signal-to-noise ratios of teleseismic receiver functions and effectiveness of stacking for their enhancement, *J. Geophys. Res.*, **108**(B2), 2106, doi:10.1029/2001JB001692.
- Neal, S. L., and G. L. Pavlis (1999), Imaging P-to-S conversions with multi-channel receiver functions, *Geophys. Res. Lett.*, **26**(16), 2581–2584.
- Owens, T. J., A. A. Nyblade, H. Gurrola, and C. A. Langston (2000), Mantle transition zone structure beneath Tanzania, East Africa, *Geophys. Res. Lett.*, **27**(6), 827–830.
- Pavlis, G. L. (2003), Imaging the Earth with passive seismic arrays, *Leading Edge*, **22**, 224–331.
- Poppeliers, C., and G. L. Pavlis (2003a), Three-dimensional, prestack, plane wave migration of teleseismic P-to-S converted phases: 1. Theory, *J. Geophys. Res.*, **108**(B2), 2112, doi:10.1029/2001JB000216.
- Poppeliers, C., and G. L. Pavlis (2003b), Three-dimensional, prestack, plane wave migration of teleseismic P-to-S converted phases: 2. Stacking multiple events, *J. Geophys. Res.*, **108**(B5), 2267, doi:10.1029/2001JB001583.
- Revenaugh, J. (1995), A scattered-wave image of subduction beneath the Transverse Ranges, *Science*, **268**, 1888–1892.
- Rondenay, S., M. G. Bostock, and J. Shragge (2001), Multiparameter two-dimensional inversion of scattered teleseismic body waves: 3. Application to the Cascadia 1993 data set, *J. Geophys. Res.*, **106**, 30,795–30,807.
- Ryberg, T., and M. Weber (2000), Receiver function arrays: A reflection seismic approach, *Geophys. J. Int.*, **141**, 1–11.
- Safar, M. H. (1985), On the lateral resolution achieved by Kirchhoff migration, *Geophysics*, **50**, 1091–1099.
- Sassolas, C., G. Lescoffit, and P. Nicodeme (1999), The benefits of 3-D ray tracing in acquisition feasibility, paper presented at 69th Annual International Meeting, Soc. of Expl. Geophys., Houston, Tex.
- Shearer, P. M., M. P. Flanagan, and M. A. H. Hedlin (1999), Experiments in migration processing of SS precursor data to image upper mantle discontinuity structure, *J. Geophys. Res.*, **104**, 7229–7242.
- Sheehan, A. F., P. M. Shearer, H. J. Gilbert, and K. G. Dueker (2000), Seismic migration processing of P-SV converted phases for mantle discontinuity structure beneath the Snake River Plain, western United States, *J. Geophys. Res.*, **105**, 19,055–19,065.
- Sheriff, R. E., and L. P. Geldart (1995), *Exploration Seismology*, 2nd ed., 392 pp., Cambridge Univ. Press, New York.
- Shragge, J., M. G. Bostock, and S. Rondenay (2001), Multiparameter two-dimensional inversion of scattered teleseismic body waves: 2. Numerical examples, *J. Geophys. Res.*, **106**, 30,783–30,793.
- Stoffa, P. L., J. T. Fokkema, R. M. de Luna Freire, and W. P. Kessinger (1990), Split-step Fourier migration, *Geophysics*, **55**, 410–421.
- Stolt, R. H. (1978), Migration by Fourier transform, *Geophysics*, **43**, 23–48.
- Vermeer, G. J. O. (1998), Factors affecting spatial resolution, *Leading Edge*, **17**, 1025–1029.
- Wang, X., et al. (Eds.) (2000), *Tan-Lu Fault Zone*, Geol. Press, Beijing.
- Wen, L., and D. V. Helmberger (1998), A two-dimensional P-SV hybrid method and its application to modeling localized structures near the coremantle boundary, *J. Geophys. Res.*, **103**, 17,901–17,918.
- Wu, R. S., and L. Chen (2001), Beamlet migration using Gabor-Daubeshies frame propagator, paper presented at 63rd Conference and Technical Exhibition, Eur. Assoc. of Geosci. and Eng., Amsterdam, Netherlands.
- Wu, R. S., and L. Huang (1992), Scattered field calculation in heterogeneous media using the phase-screen propagator, paper presented at 62nd Annual International Meeting, Soc. of Expl. Geophys., New Orleans, La.
- Wu, R. S., S. Jin, X. B. Xie, and C. C. Mosher (2000a), 2D and 3D generalized screen migrations, paper presented at 62nd Conference and Technical Exhibition, Eur. Assoc. of Geosci. and Eng., Glasgow, U.K.
- Wu, R. S., Y. Wang, and J. H. Gao (2000b), Beamlet migration based on local perturbation theory, 70th Annual International Meeting, Soc. of Expl. Geophys., Calgary, Alberta, Canada.
- Xie, X. B., and R. S. Wu (1998), Improve the wide angle accuracy of the screen method under large contrast, 68th Annual International Meeting, Soc. of Expl. Geophys., New Orleans, La.
- Xie, X. B., and R. S. Wu (2001), Modeling elastic wave forward propagation and reflection using complex screen method, *J. Acoust. Soc. Am.*, **109**, 2629–2635.
- Zhu, L. (2000), Crustal structure across the San Andreas Fault, southern California from teleseismic converted waves, *Earth Planet. Sci. Lett.*, **179**, 183–190.

L. Chen and T. Zheng, Seismological Laboratory, Institute of Geology and Geophysics, Chinese Academy of Sciences, Beijing 100029, China. (lchen@mail.igcas.ac.cn)

L. Wen, Department of Geosciences, State University of New York at Stony Brook, Stony Brook, NY 11794, USA.